

## Properties of HHFW electron heating generated H-modes in NSTX\*

J.C. Hosea<sup>1</sup>, J-W Ahn<sup>2</sup>, R.E. Bell<sup>1</sup>, C. Domier<sup>3</sup>, A. Diallo<sup>1</sup>, E. Fredrickson<sup>1</sup>, T.K. Gray<sup>2</sup>, S. Kaye<sup>1</sup>, B.P. LeBlanc<sup>1</sup>, K.C. Lee<sup>3</sup>, R. Maingi<sup>2</sup>, E. Mazzucato<sup>1</sup>, A. McLean<sup>2</sup>, C.K. Phillips<sup>1</sup>, Y. Ren<sup>1</sup>, L. Roquemore<sup>1</sup>, P.M. Ryan<sup>2</sup>, G. Taylor<sup>1</sup>, K. Tritz<sup>4</sup>, J.R. Wilson<sup>1</sup>, and the NSTX Team

<sup>1</sup>Princeton Plasma Physics Laboratory, Princeton, NJ 08543, USA

<sup>2</sup>Oak Ridge National Laboratory, Oak Ridge, TN 37831, USA

<sup>3</sup>University of California Davis, Davis, CA 95616, USA

<sup>4</sup>Johns Hopkins University, Baltimore, MD 21218, USA

### Introduction

On ITER all of the auxiliary heating methods will primarily heat in the electron channel [1] (electron cyclotron heating ECH, neutral beam injection NBI, ion cyclotron heating ICH, lower hybrid heating LHH, and fusion product heating) and therefore it is of considerable interest to determine the properties of H-mode plasmas generated with electron heating in the absence of positive NBI in existing devices. On NSTX, plasma conditioning of the high harmonic fast wave (HHFW) antenna to remove lithium deposits [2], which can be sputtered into the interior of the Faraday shield enclosures and result in arcing at the antenna elements [3], has allowed the HHFW power  $P_{RF}$  to be raised above the threshold for the RF only H-

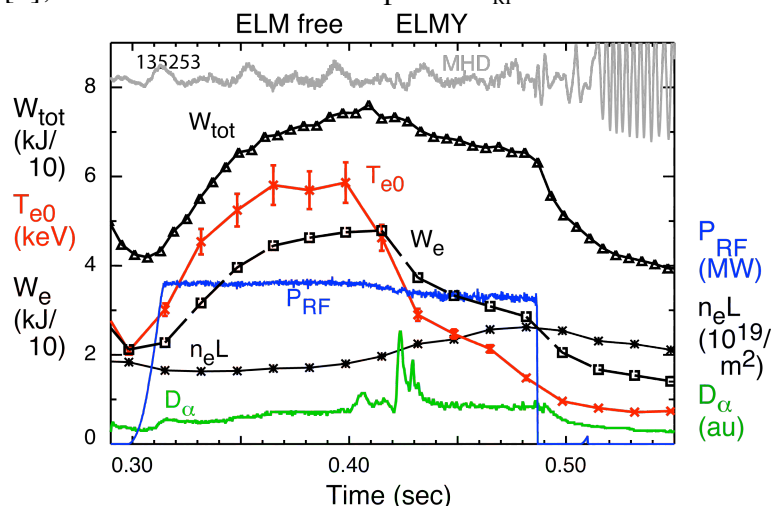


**Figure 1.** Discharge characteristics for the H-mode produced with  $P_{RF} \sim 3.7$  MW. ( $B_T = 0.55$  T,  $I_p = 0.65$  MA, helium,  $k_{||} = -8\text{m}^{-1}/\phi_{Ant} = -90^\circ$ ). The ELM-free-like and ELMv phases are denoted.

localized oscillations leading into small ELMs, followed by an ELMy phase with large ELMs. During the ELM-free-like phase, both the total and electron stored energies increase substantially and  $T_e(0)$  is sustained in the 5 – 6 keV range. The stored energies and  $T_e(0)$

mode [4] ( $P_{RF} \sim 2.5$  MW for  $n_e \sim 2 \times 10^{19}\text{m}^{-3}$ ,  $B_T = 0.55$  T,  $I_p = 0.65$  MA, helium). In this paper some of the properties of ELM-free-like and ELMy HHFW H-modes are presented.

As shown in Fig. 1 for  $P_{RF} \sim 3.7$  MW, HHFW H-modes exhibit an ELM-free-like phase, with small edge

decrease markedly with the onset of the large ELMs as is also generally observed for NBI generated H-modes.

### Properties of HHFW generated ELMs

A fast infrared (IR) camera has been used to measure the heat flux deposited on the lower divertor tiles [5] for the conditions of Fig. 1. Figure 2a shows the heat fluxes for 4 radii starting at  $R = 0.562$  m, the outer divertor strike radius, and progressing outward in  $R$  to  $R = 0.975$  m (corresponding to a projected  $R$  of  $\sim 156$  cm at the plasma midplane,  $\sim 2$  cm in front of the antenna surface). It is clear that the heat flux is enhanced during the ELM-free-like phase and even more so during the ELM phase. Also, the heat flux is strongly peaked in the vicinity of the outer strike radius in both phases. This is quite evident in Fig. 2b where the heat fluxes at the time of the largest ELM and the time of the minimum in heat flux preceding it are plotted versus  $R$ . Also, subtraction of the background flux reveals the ELM deposition is even more peaked about the outer strike radius -  $\sim 10$  MW/m<sup>2</sup> with a half flux width of  $\sim 1$  cm

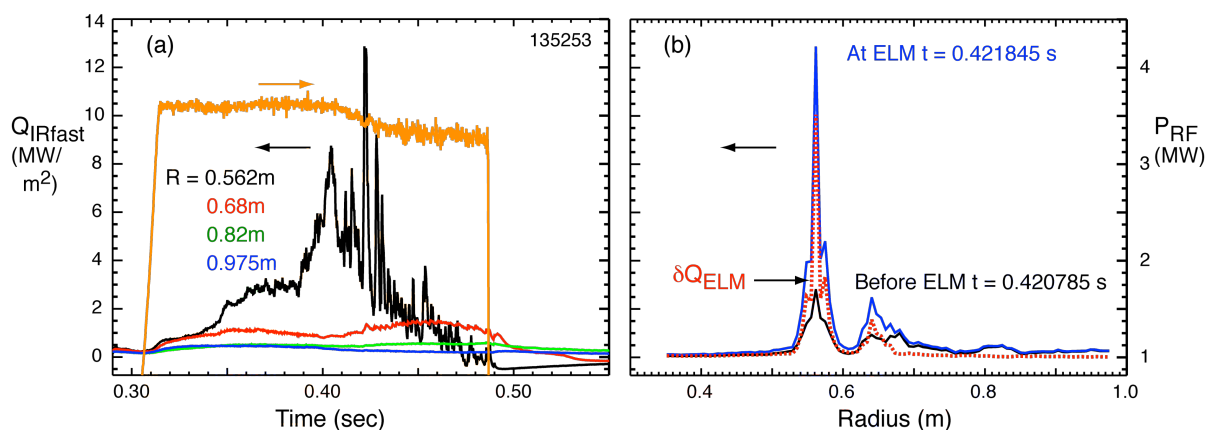


**Figure 2.** Fast IR measurements of heat flux at Bay H versus (a) time for 4 major radii at the divertor tiles and (b) major radius at the time of the largest ELM and at the minimum preceding it. (Conditions of Fig. 1.)

– and falls off by two orders of magnitude as  $R$  approaches 1 m. This peaking is much stronger than typically observed for the NBI+HHFW ELMy H-modes at a similar total power ( $\sim 0.3$  MW/m<sup>2</sup> with a  $\sim 21$  cm half flux width at  $P_{\text{NB}} \sim 2$  MW and  $P_{\text{RF}} \sim 1.9$  MW [6]).

The strong fall off of the ELM heat flux deposition with radius is consistent with the very small effect that the ELM has on the antenna loading – the dip in  $P_{\text{RF}}$  for the largest ELM in Fig. 2a is only  $\sim 3\%$  even though the plasma-antenna gap is only  $\sim 3$  cm at the time of the ELM.

If such strong peaking of the heat flux deposition in the vicinity of the outer strike radius should occur for electron heating generated H-modes on ITER (e.g., with ECH), it may be necessary to sweep the strike radius to avoid excessive tile erosion. However, a startup

scenario employing ICH heating of an ECH generated H-mode having a small plasma-antenna gap might prove to be attractive.

It would appear that the absence of energetic ions for the HHFW H-mode on NSTX is responsible for the very focused ELM heat flux deposition pattern about the outer strike radius. This possibility should be investigated for the ECH ELMy H-mode regime as well [1, 7] to determine if this is a general result for the electron heating generated H-mode.

### Transport properties during the ELM-free-like H-mode phase

It is observed that the stored energies achieved during the ELM-free-like phase at a reduced power of  $P_{RF} \sim 2.7$  MW saturate at about the same levels as for  $P_{RF} \sim 3.7$  MW (Fig. 1) as shown in Fig. 3a. Note that at this lower power the ELM-free-like phase starts at  $t \sim 0.36$  sec and the evolution of edge oscillations into small ELMs and ultimately a large ELM is tracked by the edge soft x-ray signal with no filter [8]. When  $P_{RF}$  is programmed up to  $\sim 3.7$  MW, held at this power for 50 msec, and then programmed to fall to zero slowly in time (Fig. 3b), the start of the ELM-free-like phase begins near the end of the constant power flat-top and it persists throughout the fall off in power down to  $P_{RF} \sim 1.3$  MW, where it terminates in a large ELM. Again the stored energies saturate during the  $P_{RF}$  ramp down in Fig. 3b at about

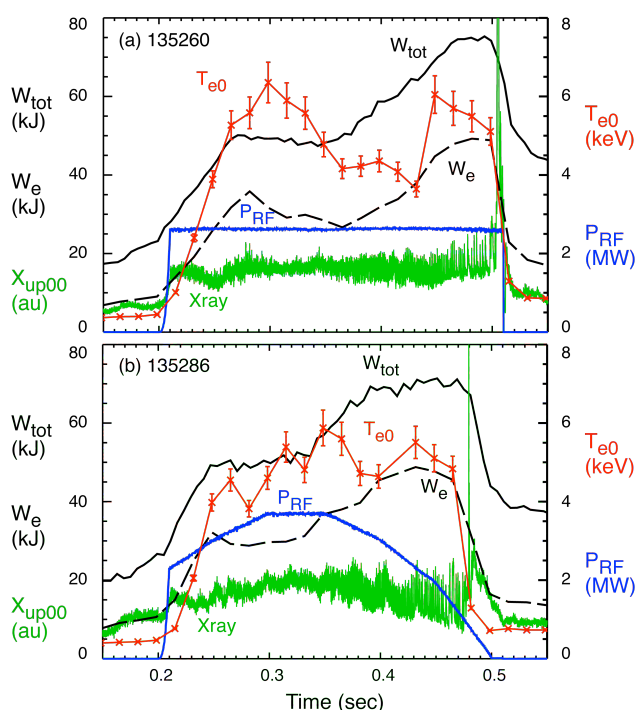


**Figure 3.** Stored energy during the ELM-free-phase for (a) a constant  $P_{RF} \sim 2.7$  MW, and (b) a programmed  $P_{RF}$  which falls from  $P_{RF} \sim 3.7$  MW to zero in  $\sim 150$  msec. ( $B_T = 0.55$  T,  $I_p = 0.65$  MA, helium,  $k_{||} = -8m^{-1}/\phi_{Ant} = -90^\circ$ .)

the same levels as in Figs. 1 and 3a. These observations indicate that turbulent transport is adjusting to the core RF power level to keep the electron pressure profiles stiff.

Thomson scattering profiles are shown in Fig. 4a for the saturated conditions of Fig. 1 (3.7 MW at 0.380 sec) and of Fig. 3a (2.7 MW at 0.482 sec). The electron density profiles for these cases are quite similar and the electron temperature and pressure profiles almost overlay. Note that the  $T_e$  pedestal is at  $\sim 250$  eV similar to the level observed for central ECH heating on DIII-D [9]. The temperature gradients at the radius

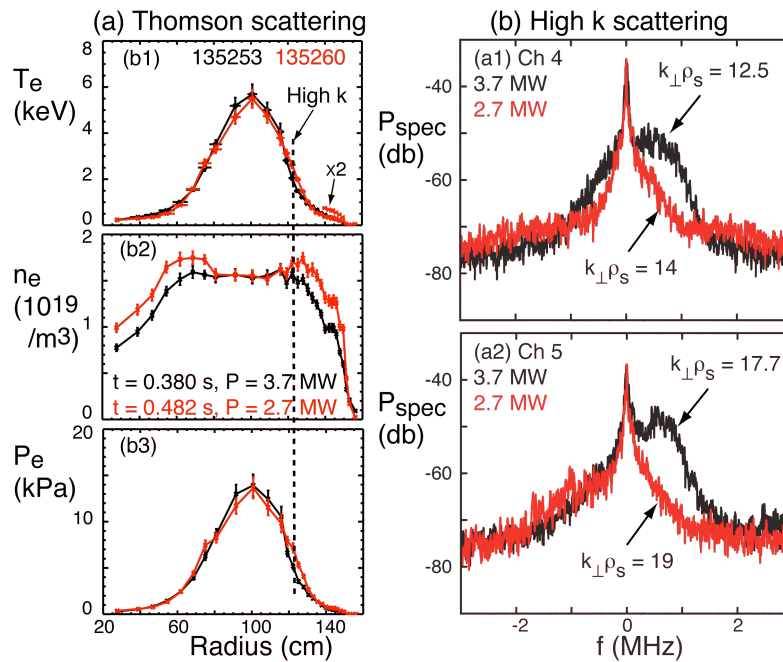


**Figure 4.** (a) Thomson scattering profiles and (b) high-k scattering spectra for Fig. 1 (3.7 MW) at 0.380 sec and Fig. 3a (2.7 MW) at 0.482 sec.

of  $R \sim 1.23$  m (dashed line in Fig. 4a). It is found that the turbulence spectra are reduced over an order of magnitude for the two high-k scattering channels employed [12] when the power is reduced from 3.7 MW to 2.7 MW.

## References

1. R. Prater *et al.*, *Bulletin APS* **54** (2009) NO4 11. [[https://diii-d.gat.com/diii-d\\_global/presentations/dpp2009/Prater.pdf](https://diii-d.gat.com/diii-d_global/presentations/dpp2009/Prater.pdf)]
2. G. Taylor *et al.*, *Physics of Plasmas* **17**, (2010) 056114.
3. J.C. Hosea *et al.*, *AIP Conf Proceedings* **1187** (2009) 105.
4. S. Kaye, R. Maingi, D. Battaglia, *et al.*, IAEA Fusion Energy Conf. (Daejeon, 2010) paper EXC/2-3Rb.
5. J-W. Ahn *et al.*, *Review of Scientific Instruments* **81** (2010)
6. J.C. Hosea *et al.*, *RF Conference* (2011, Newport).
7. J.S. deGrassie *et al.*, *Physics of Plasmas* **11** (2004) 4323.
8. R. Maingi *et al.*, *Nuclear Fusion* **45** (2005) 264.
9. J. Lohr *et al.*, *Physical Review Letters* **60** (1988) 2630.
10. H. Yuh *et al.*, *Physical Review Letters* **106** (2011) 055003.
11. E. Mazzucato *et al.*, *Nuclear Fusion* **49** (2009) 055001.
12. D.R. Smith *et al.*, *Review of Scientific Instruments* **75** (2004) 3840.

\* This manuscript has been authored by Princeton University under Contract Number DE-AC02-09CH11466 with the U.S. Department of Energy. The publisher, by accepting this article for publication, acknowledges that the United States Government retains a non-exclusive, paid-up, irrevocable, world-wide license to publish or reproduce the published form of this manuscript, or allow others to do so, for United States Government purposes.

denoted by the dashed vertical line fall in the range of  $R/L_{Te} = R \cdot d \ln Te/dr \sim 6 - 8$ , which exceeds the critical temperature gradient of the ETG mode typical for a monotonic  $q$  profile [10], and thus such high-k turbulence may be controlling the transport.

That the high-k turbulence possibly caused by the ETG mode [11] is a strong function of the RF power level is shown in Fig. 4b for a radial location